Structure
Article

Structures of SMG1-UPFs Complexes: SMG1 Contributes to Regulate UPF2-Dependent Activation of UPF1 in NMD

Roberto Melero,[1,4] Akiko Uchiyama,[2,4] Raquel Castaño,[1] Naoyuki Kataoka,[3] Hitomi Kurosawa,[2] Shigeo Ohno,[2] Akio Yamashita,[2,*] and Oscar Llorca[1,*]
[1]Centro de Investigaciones Biológicas, Consejo Superior de Investigaciones Científicas (Spanish National Research Council), Ramiro de Maeztu 9, 28040 Madrid, Spain
[2]Department of Molecular Biology, Yokohama City University School of Medicine, 3-9, Fukuura, Kanazawa-ku, Yokohama, Kanagawa 236-0004, Japan
[3]Medical Innovation Center, Laboratory for Malignancy Control Research, Kyoto University Graduate School of Medicine, 53, Shogoin Kawaharacho, Sakyo-ku, Kyoto 606-8507, Japan
[4]Co-first author
*Correspondence: yamasita@yokohama-cu.ac.jp (A.Y.), ollorca@cib.csic.es (O.L.)
http://dx.doi.org/10.1016/j.str.2014.05.015

SUMMARY

SMG1, a PI3K-related kinase, plays a critical role in nonsense-mediated mRNA decay (NMD) in mammals. SMG1-mediated phosphorylation of the UPF1 helicase is an essential step during NMD initiation. Both SMG1 and UPF1 are presumably activated by UPF2, but this regulation is incompletely understood. Here we reveal that SMG1C (a complex containing SMG1, SMG8, and SMG9) contributes to regulate NMD by recruiting UPF1 and UPF2 to distinct sites in the vicinity of the kinase domain. UPF2 binds SMG1 in an UPF1-independent manner in vivo, and the SMG1C-UPF2 structure shows UPF2 recognizes the FRB domain, a region that regulates the related mTOR kinase. The molecular architectures of several SMG1C-UPFs complexes, obtained by combining electron microscopy with in vivo and in vitro interaction analyses, competition experiments, and mutations, suggest that UPF2 can be transferred to UPF1 within SMG1C, inducing UPF2-dependent conformational changes required to activate UPF1 within an SMG1C-UPF1-UPF2 complex.

INTRODUCTION

SMG1 kinase is a large protein (410 kDa) that belongs to the phosphatidylinositol (PI) 3-kinase-related kinase (PIKK) family. PIKKs comprise six members in mammals including mammalian target of rapamycin (mTOR), DNA-dependent protein kinase catalytic subunit (DNA-PKcs), ataxia telangiectasia mutated (ATM), and ATM- and Rad3-related (ATR) kinases (Izumi et al., 2012; Yamashita, 2013; Yamashita et al., 2001). Structural analysis using X-ray crystallography and electron microscopy (EM) of several kinases in the PIKK family including SMG1, revealed that the entire C terminus containing three conserved regions, the FRAP, ATM, and TRRAP (FAT) domain followed by a catalytic domain with homology to PI3-kinases (PIKK domain hereafter) and ending in a short FAT C-terminal (FATC) domain (Figure 1A), forms a globular region (Figures 1B and 1C) (Arias-Palomo et al., 2011; Sibanda et al., 2010; Yang et al., 2013). The N terminus in all PIKKs is made of a long stretch of helical repeats, mostly the huntington, elongation factor 3, A subunit of PP2A, and TOR1 (HEAT) repeats, forming a helical scaffold that is thought to be involved in protein binding, which protrudes from the globular C terminus, as revealed in the crystal structure of DNA-PKcs (Sibanda et al., 2010) (Figure 1C). SMG1 also contains a unique long insertion between the catalytic and FATC domains, but the function of this region is not understood. In addition, a 100-residue FKBP12-rapamycin-binding (FRB) domain, positioned between the FAT and PIKK, has been described for some but not all PIKKs, including mTOR and SMG1 (Yang et al., 2013). The atomic structure of the 1,500-amino acid C-terminal region of mTOR revealed that the FRB regulates the access of substrates to the active site of the kinase domain (Yang et al., 2013) (Figure 1B).

SMG1 forms the so-called SMG1 complex (SMG1C) with SMG8 and SMG9 and plays an essential role in an mRNA quality control mechanism called nonsense-mediated mRNA decay (NMD) by phosphorylating UPF1, a central regulator of NMD. UPF1 is an RNA helicase containing two RecA-like domains in tandem at its C terminus (Chakrabarti et al., 2011; Clerici et al., 2009). In its closed conformation, an N-terminal cysteine-histidine-rich (CH) domain inhibits the helicase activity (Chakrabarti et al., 2011). NMD targets transcripts harboring premature termination codons (PTCs) resulting from germline mutations in many genetic disorders and during mRNA processing (Kervestin and Jacobson, 2012; Schweingruber et al., 2013; Yamashita, 2013). NMD is also estimated to regulate expression of a significant fraction of physiological mRNAs (Hansen et al., 2009; Mendell et al., 2004; Weischenfeldt et al., 2012).

In a current model of PTCs recognition in mammals, aberrant translation termination induces the interaction of UPF1 with the terminating ribosome to assemble a complex containing UPF1, release factors eRF1 and eRF3, and SMG1, known as the SMG1-UPF1-eRF1-eRF3 (SURF) complex (Kashima et al., 2006). The SURF complex forms independently of UPF2, and

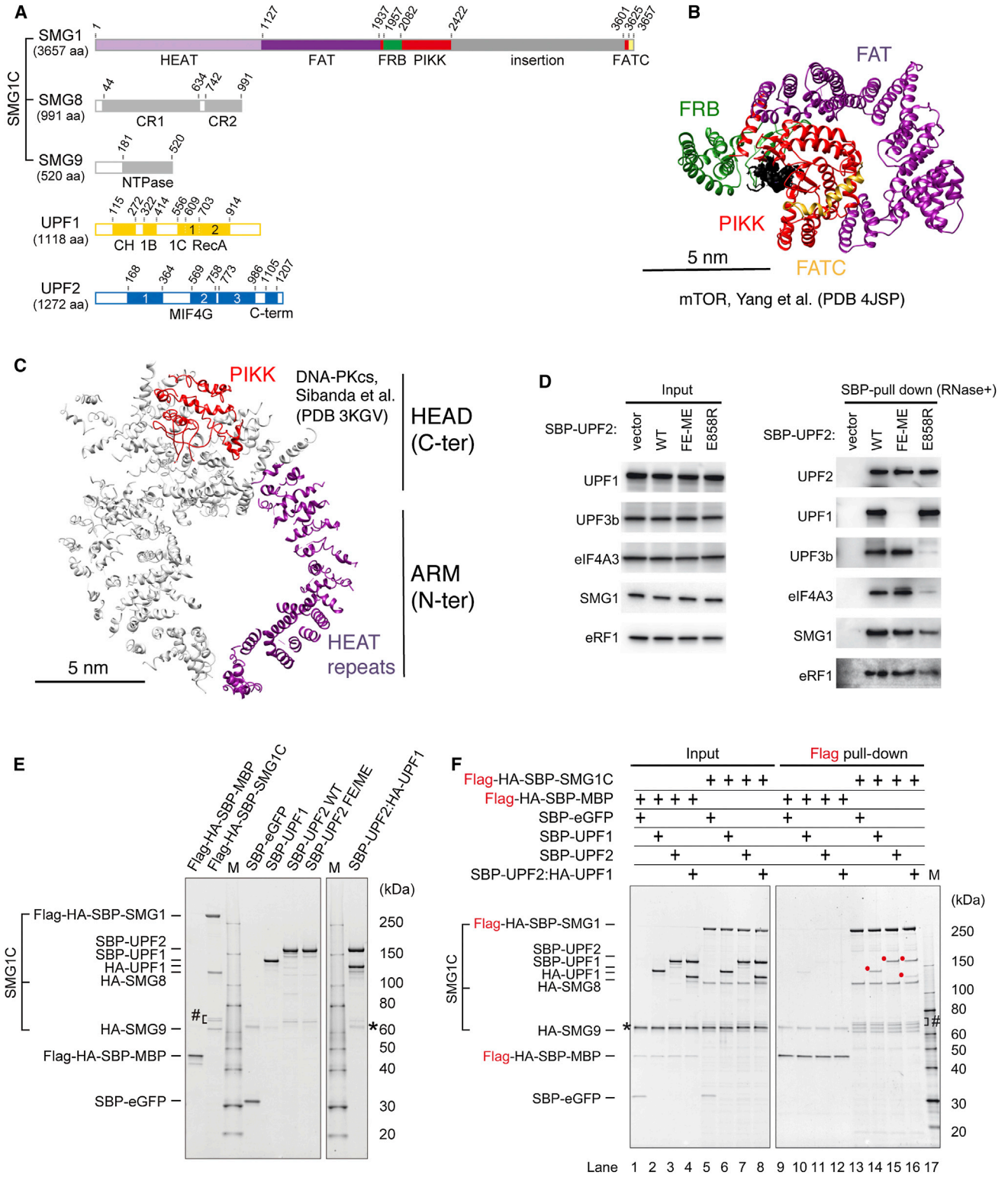

Figure 1. In Vitro Reconstitution of SMG1C-UPF1, SMG1C-UPF2, and SMG1C-UPF1-UPF2

(A) Schematic representation of SMG1, SMG8, SMG9, UPF1, and UPF2 used in this study. Color codes and abbreviations for each domain are maintained throughout the figures. Individual domains of SMG1 (HEAT repeats in light purple; FAT domain in dark purple; FRB domain in green; PIKK domain in red; SMG1 specific insertion in gray; FATC domain in pale yellow), SMG8 (two conserved regions among metazoans CR1 and CR2 in gray), SMG9 (NTPase domain in gray), UPF1 (CH, 1B, and 1C domains, and two RecA-like domains RecA1 and RecA2 in yellow), and UPF2 (three predicted MIF4G domains MIF4G1, MIF4G2, and MIF4G3 and the C-terminal region in blue) are indicated.

(legend continued on next page)

the SMG1 activity in SURF is downregulated by SMG8 and SMG9 (Yamashita et al., 2009; Arias-Palomo et al., 2011). If an exon junction complex (EJC) is located 50–55 or more nucleotides downstream from the termination codon, the SURF complex physically associates with the downstream EJC through UPF2 and UPF3, two evolutionally conserved NMD factors. The association between SURF and UPF2-UPF3-EJC would induce SMG1-mediated UPF1 phosphorylation (Kashima et al., 2006; Yamashita et al., 2009). Phosphorylated UPF1 recruits phopho-UPF1 recognizing protein complexes that can degrade PTC-mRNA (Glavan et al., 2006; Loh et al., 2013; Okada-Katsuhata et al., 2012). In addition, binding of UPF2 to the CH domain of UPF1 induces a large conformational change that removes the inhibition of the ATPase activity and activates the RNA-dependent 5′ to 3′ helicase activity of UPF1(Clerici et al., 2009). This helicase activity is thought to be required to strip the mRNP of proteins (Franks et al., 2010) and/or to bridge the distance between the stalled ribosome and a downstream EJC (Shigeoka et al., 2012).

SMG1-mediated UPF1 phosphorylation is an essential step in NMD. It has been shown that overproduction of wild-type SMG1 induced the accumulation of phosphorylated UPF1 and enhanced mRNA decay, whereas overproduction of kinase inactive SMG1 reduced the amount of phosphorylated UPF1 and suppressed mRNA decay (Yamashita et al., 2001). Despite its relevance, the regulation of SMG1 kinase and how the UPF1-UPF2 complex regulates SMG1 are poorly understood. The recruitment of substrates to the kinase domain seems to be the main mechanism controlling phosphorylation by mTOR (Yang et al., 2013), but this model cannot be directly extrapolated to SMG1 because UPF2 and UPF3 are required to activate UPF1 phosphorylation by SMG1 in vivo (Ivanov et al., 2008; Kashima et al., 2006). Here we provide insights into the structural basis of NMD initiation. We have studied the architecture of several complexes between SMG1C, UPF1, and UPF2. We reveal that SMG1C could coordinate NMD initiation by recruiting UPF1 and UPF2 to nearby positions, facilitating their access to the kinase domain as well as their interaction to promote a helicase-active conformation of UPF1.

RESULTS

UPF2 Binds SMG1 in an UPF1-Independent Manner in Vivo

SMG1 forms a complex with UPF1 in an UPF2-independent manner as part of SURF (Kashima et al., 2006), which we confirmed here (see below). We evaluated the UPF1-independent binding of UPF2 to SMG1 in vivo using streptavidin-binding peptide (SBP)-tagged versions of wild-type UPF2, UPF2-F1113E-M1173E (UPF2-FE/ME hereafter), which is expected to bind UPF1 poorly (Clerici et al., 2009), and UPF2-E858R, which is affected on UPF3 binding (Kadlec et al., 2004; Kashima et al., 2006) in HeLa TetOff cells (Figure 1D). Wild-type SBP-UPF2 precipitated SMG1, UPF1, UPF3b, eRF1, and eIF4A3, whereas SBP-UPF2-E858R bound UPF1 but not UPF3b. SBP-UPF2-FE/ME also precipitated SMG1 but failed to bind UPF1, confirming that SMG1 can bind UPF2 independently of UPF1 in mammalian cells.

In Vitro Reconstitution of SMG1C-UPF1, SMG1C-UPF2, and SMG1C-UPF1-UPF2

We reconstituted in vitro the various complexes that can form SMG1C with UPF1 and UPF2 to determine their molecular architecture. For this, we first purified the SMG1C complex (SMG1-SMG8-SMG9), UPF1, UPF2, and a complex between UPF1 and UPF2 (Figure 1E). SMG1C was preassembled after cotransfecting full-length Flag-HA-SBP-SMG1 (residues 1–3657), HA-SMG9 (residues 2–520), and HA-SMG8 (residues 2–991), and the complex, Flag-HA-SBP-SMG1C hereafter, was obtained by affinity chromatography using the SBP tag in SMG1 as described before (Arias-Palomo et al., 2011). SMG1 activity is suppressed by SMG8 and SMG9 in this complex (Arias-Palomo et al., 2011). UPF1 (including the disordered N- and C-terminal tails) and full-length UPF2 were produced as SBP-tagged versions expressed and purified from human cells. In addition, the UPF1-UPF2 complex was preassembled after cotransfection of HA-UPF1 and SBP-UPF2.

Then we tested whether Flag-HA-SBP-SMG1C interacted with SBP-UPF1 or SBP-UPF2 using anti-Flag beads. SBP-UPF1 and SBP-UPF2 were pulled down only when Flag-HA-SBP-SMG1C was present in the input mixture (Figure 1F, lanes 14 and 15, coprecipitated proteins labeled with a red dot), compared with the experiments with Flag-HA-SBP-tagged maltose-binding protein (MBP; Figure 1F, lanes 9–12). SMG8 and SMG9 were also detected as part of the precipitated complexes, suggesting that an intact SMG1C interacts with UPF1 and UPF2, as we later confirmed by EM. In addition, we found that SMG1C could also interact with both proteins when forming the UPF1-UPF2 complex (Figure 1F, lane 16, coprecipitated proteins labeled with a red dot). In this experiment, the signals for HA-UPF1 and SBP-UPF2 were roughly similar in the input

(B) A view of the atomic structure of mTOR C-terminal domains (PDB ID 4JSP) (Yang et al., 2013) represented as ribbons. ATP is displayed as a solid black density bound to the PIKK domain. The scale bar represents 5 nm.
(C) A view of the crystal structure of DNA-PKcs (PDB ID 3KGV) (Sibanda et al., 2010) represented as ribbons. The section of the helical HEAT repeats used to fit within SMG1 and SMG1C (see below) and PIKK domain are shown. The rest of the crystal structure is shown in gray. The scale bar represents 5 nm.
(D) Pull-down assays using SBP-tagged version of UPF2 from HeLa TetOff cell lysates. Experiments were carried out using wild-type UPF2, UPF2-F1113E-M1173E, and UPF2-E858R mutants in the presence of RNase. UPF1, UPF3b, eIF4A3, SMG1, and eRF1 were detected by WB using specific antibodies for each protein.
(E) SDS-PAGE gels stained with Oriole stain of the purified proteins used in the biochemical analyses. Proteins were expressed in 293T cells and purified by streptavidin Mag Sepharose. The name at the top of the gel indicates the shortened name that will be used through the text.
(F) In vitro pull-down assay using Flag-tagged SMG1C. Flag-HA-SBP-MBP (as control) or Flag-HA-SBP-SMG1C (30 nM each) incubated with SBP-eGFP (as control), SBP-UPF1, SBP-UPF2, and SBP-UPF2:HA-UPF1 complex (90 nM each). After incubation, the mixtures were pulled down using anti-Flag beads. Precipitated materials as well as 20% of input were subjected to SDS-PAGE and stained with Oriole stain. Red dots, asterisk (*), and hash (#) indicate the position of coprecipitated proteins, BSA, and an uncharacterized contamination of Flag-HA-SBP-SMG1C, respectively.
See also Figure S1.

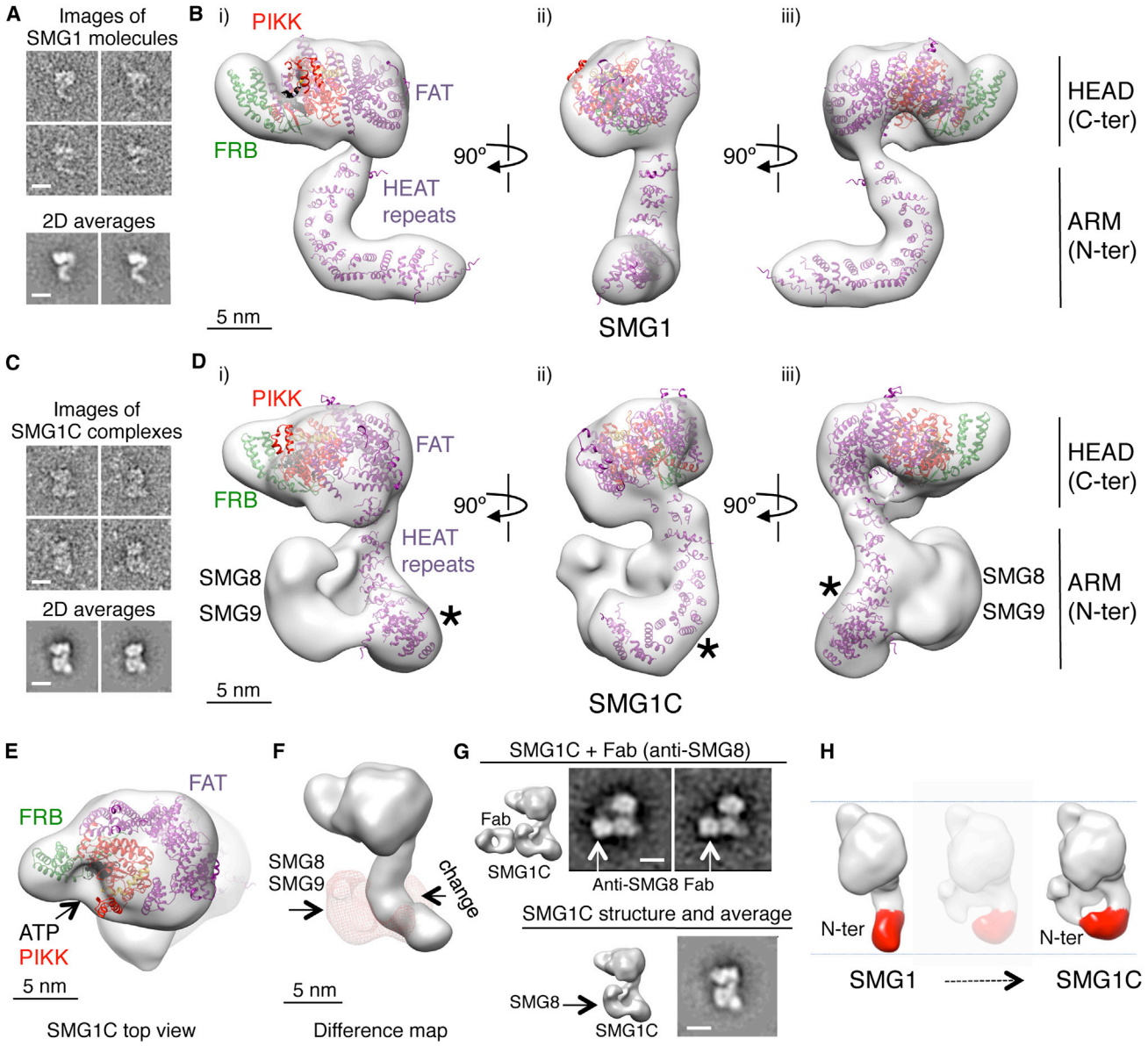

Figure 2. Molecular Architecture of SMG1 and SMG1C

(A) A gallery of four representative images of SMG1 molecules and two representative 2D averages of SMG1. The images revealed that SMG1 was structured into a compact head (at the top of each molecule in these panels) and a thinner arm (at the bottom of each molecule in these panels). The scale bar represents 10 nm.

(B) Three approximately orthogonal views (labeled i, ii, and iii) of the EM structure of SMG1 (gray transparent density) fitted with a HEAT repeat segment of DNA-PKcs (PDB ID 3KGV) (Sibanda et al., 2010) and the catalytic region of mTOR crystal structures (PDB ID 4JSP) (Yang et al., 2013). Domains are named and colored as described in Figure 1A. The scale bar represents 5 nm.

(C) A gallery of four representative images of SMG1C complexes and two representative 2D averages of SMG1C. The scale bar represents 10 nm.

(D) Three approximately orthogonal views (labeled i, ii, and iii) of the EM structure of SMG1C (gray transparent density). Domains are named and colored as described in (B). To facilitate the comparison, the three views of SMG1C represent a roughly similar orientation to that of SMG1 in the corresponding top panel. The SMG1C view in (i) is slightly tilted compared to the corresponding view of SMG1 to facilitate the observation of SMG8-SMG9 bound to SMG1. Asterisks (*) indicate those regions of SMG1C where the arm has rotated compared to its position in SMG1. The scale bar represents 5 nm.

(E) A top view of SMG1C represented as in (D) highlighting the location of several domains.

(F) Difference map obtained after subtracting the structure of SMG1 to SMG1C. The difference is shown as a grid represented on the structure of SMG1. This difference maps SMG8-SMG9 in SMG1C and a conformational change.

(G) 2D averages of several images of immunocomplexes resulting from the incubation of SMG1C with anti-SMG8 Fab fragments. The immunocomplexes showed a similar structure than SMG1C, but a density of dimensions compatible with a Fab was detected in contact with SMG1C. To help comparisons, a view of the 3D structure and a 2D average of SMG1C and a view of a 3D model of a Fab fragment bound to SMG1C are shown. The scale bar of the EM images represents 10 nm.

(legend continued on next page)

material, as expected for a 1:1 complex, but SBP-UPF2 was recovered more efficiently than HA-UPF1 in the precipitate. Overall our data indicated that SMG1C could interact with UPF1, UPF2, and also with an UPF1-UPF2 complex.

We next explored the structural basis for these interactions by reconstituting several SMG1C-UPFs complexes in vitro and determining their structure using EM (see below). For all structural analysis, we purified highly homogenous protein preparations (Figure S1A available online), and complexes were assembled in vitro by incubating purified SMG1C with an excess of UPF1, UPF2, or UPF1-UPF2. Mixtures were analyzed by EM (Figures S1B–S1H). The final yield of purified complexes was low, precluding the preparation of vitrified specimens but sufficient for a study using negative staining. We also observed that a mild stabilization of the interactions using 0.02% glutaraldehyde significantly improved the yield of images corresponding to SMG1C-UPFs. For all complexes, we used image processing and classification techniques to sort out all images into subsets corresponding to homogenous structural species. Those images corresponding to SMG1C-UPFs complexes were identified and used to determine their 3D structures (details in Experimental Procedures).

SMG1 Is Regulated by Large Conformational Changes

We first defined the molecular architecture of SMG1 and SMG1C, resolved at ~21 Å resolution (Figure 2), required to interpret the structures of the SMG1C-UPFs complexes. The structure of SMG1 comprised a globular "head" region and a thinner "arm," which our modeling revealed to correspond to the C- and N-terminal segments of the protein, respectively (Figures 2A and 2B). The atomic structure of the C-terminal domains mTOR (Yang et al., 2013) fitted extraordinarily well within the head (cross correlation = 0.90), and we obtained only one high correlating solution due to constrains during the fitting experiment introduced by a protrusion at the EM structure assigned to the FRB domain (Figures 2A and 2B). Thus, the SMG1 head comprises the C-terminal region of the protein, and the catalytic PIKK, FAT, FRB, and FATC domains were located in their approximate positions by comparison with mTOR. The SMG1 specific insertion connects the PIKK and FATC domains (Figure 1A), but this region is not present in mTOR (Yang et al., 2013). Predictions of secondary structure suggested that the SMG1-specific insertion contains several large α helices (not shown), but the confidence values for these predictions were low. Nonetheless, they were an indication suggesting that this domain is probably mostly folded. We evaluated whether the 3D structure of SMG1 could accommodate the SMG1-specific insertion in the C terminus (Figure S2). Our analysis revealed that the atomic structure of mTOR did not justify all the density at the head of SMG1, and there is probably sufficient density left to fit the SMG1-specific insertion (Figure S2). The SMG1 arm could be fitted with a defined HEAT repeat segment (Figure 2B) corresponding to the predicted N-terminal end of the 6.6 Å resolution crystal structure of DNA-PKcs (cross correlation = 0.93) (Sibanda et al., 2010).

The head of SMG1C was roughly similar to SMG1 (Figures 2C and 2D), and the active site formed a cleft with the FRB domain located in the vicinity as in mTOR (Yang et al., 2013) (Figure 2E). SMG8 and SMG9 were mapped in SMG1C after aligning and subtracting the structure of SMG1 to SMG1C (Figure 2F). The difference map revealed a small difference in the arm region because of conformational changes (see below), and a major density corresponding to the SMG8-SMG9 complex. SMG9 is required to recruit SMG8 to SMG1C (Arias-Palomo et al., 2011), suggesting that SMG9 probably locates in closer contact with SMG1 within the SMG8-SMG9 density. SMG8 was mapped at the other end by immunolabeling using Fab fragments derived from polyclonal antibodies targeting SMG8 (Figure 2G). The comparison of SMG1 with SMG1C reveals that the interaction of SMG8-SMG9 with SMG1 induces a large rotation in the N-terminal end of the HEAT repeats arm region (Figure 2D, labeled with asterisks; Figure 2H; Movies S1 and S2).

SMG1C Positions UPF1 in the Proximity of the PIKK Domain

We next reconstituted a complex containing SMG1C and UPF1 by incubating SMG1C (71 nM final concentration) and an excess of UPF1 (1:5 molar ratio), and the mixture was observed in the electron microscope and analyzed by image processing (Figure 3A and Figure S1). UPF1 appeared in the electron microscope as a roughly square-shaped density with several lobes, as could be expected for the closed conformation (Chakrabarti et al., 2011) (Figure 3B). A density of similar dimensions was consistently positioned in contact with a distinct region of SMG1C in 40% of the images in the data set, which was interpreted as UPF1 binding to a defined site of SMG1C (Figures 3A and 3B). Similar images of the complex, but with a significantly improved yield (63%), were obtained after a mild stabilization with 0.02% glutaraldehyde (Figure 3B).

UPF1 was mapped within the 3D structure of SMG1C-UPF1 and solved at ~21 Å resolution (Figures 3C and 3D) by aligning and subtracting the structure of SMG1C to SMG1C-UPF1 (Figure 3E). The comparison of SMG1C and SMG1C-UPF1 also allowed extrapolating the structural model for SMG1C to SMG1C-UPF1. UPF1 binds to regions in the proximities of the PIKK domain (Figures 3C and 3D), in a conformation more similar to the closed conformation described in the crystal structure of the helicase-inhibited UPF1 than the open conformation (cross correlations = 0.92 versus 0.75) (Chakrabarti et al., 2011; Clerici et al., 2009) (Figure 3E). The limited resolution precluded the description of a precise orientation of UPF1 within the complex to define what part of UPF1 contacts SMG1. Thus, we analyzed the interaction of two purified SBP-tagged fragments comprising residues 2–295 (corresponding to the CH domain) and residues 291–1118 (including the two RecA-like domains) of UPF1 with SMG1 (Figure S3). We detected a weak but significant

(H) The interaction of SMG8-SMG9 to SMG1 induced a large clockwise rotation of the arm, highlighted in red within the EM structures of SMG1 and SMG1C shown in gray. The movement that could take place from SMG1 to SMG1C was modeled, and the figure represents several hypothetical transient states. SMG1 and SMG1C are showed slightly tilted to help visualizing the conformational change. A full movie can be seen in Movie S1.
See also Figure S2.

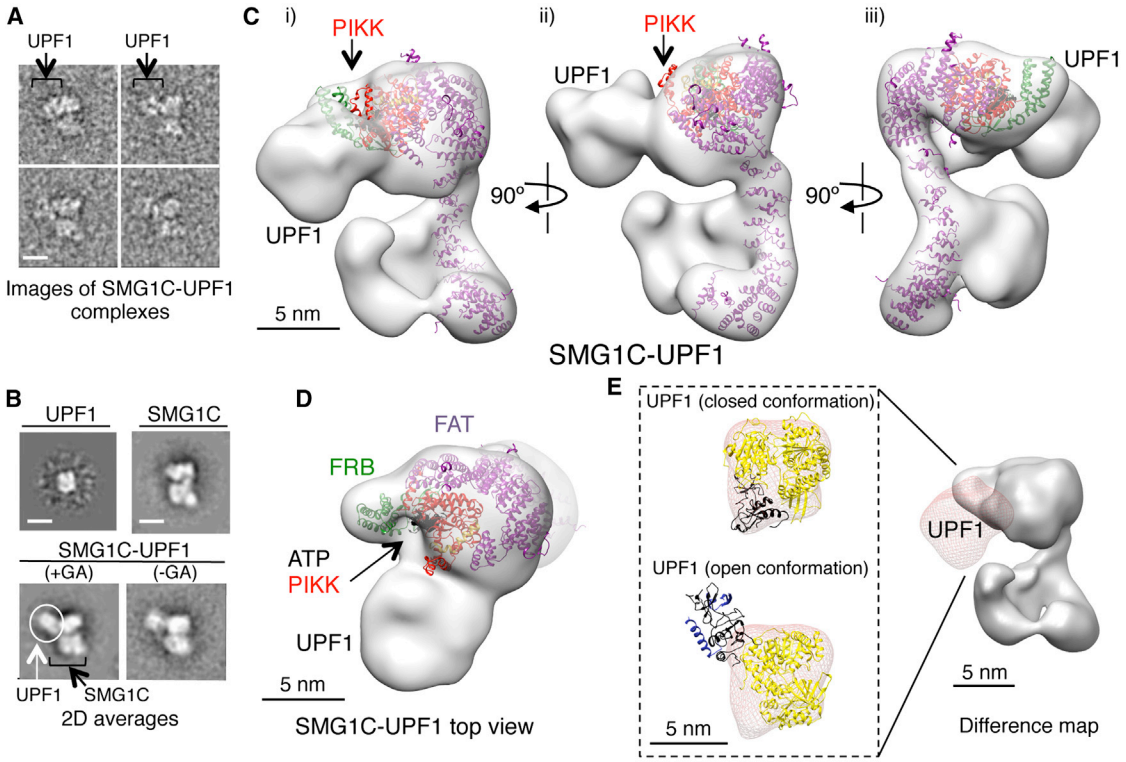

Figure 3. Structure of SMG1C-UPF1

(A) A gallery of four representative images of SMG1C-UPF1 complexes. The scale bar represents 10 nm.

(B) Representative 2D averages of UPF1, SMG1C, and SMG1C-UPF1. Averages of SMG1C-UPF1 obtained before and after a mild stabilization with glutaraldehyde (GA) are shown. The comparison of SMG1C, UPF1, and SMG1C-UPF1 identified UPF1 as a density bound to the head of SMG1, which has been highlighted within a circle. The scale bar represents 10 nm.

(C) Three approximately orthogonal views (labeled i, ii, and iii) of the EM structure of SMG1C-UPF1 (gray transparent density) fitted with segments of DNA-PKcs (Sibanda et al., 2010) and mTOR (Yang et al., 2013). The scale bar represents 5 nm.

(D) A top view of the SMG1C-UPF1 complex represented as in (C).

(E) Difference map obtained after subtracting SMG1C to SMG1C-UPF1, represented as a grid on the structure of SMG1C. The difference locates UPF1 in the complex, and this density was fitted with the crystal structures of UPF1 in the closed and open conformations (Chakrabarti et al., 2011; Clerici et al., 2009).

interaction of SBP-UPF1$^{291–1118}$ with Flag-HA-SBP-SMG1C (Figure 4A). This result was confirmed after detecting the interaction of SBP-UPF1$^{291–1,118}$ with MBP-SMG1$^{1808–2743}$ (residues 1808–2743, comprising the FRB and PIKK domains, and part of the SMG1-specific insertion) (Figure 4B). Together, these results suggested that UPF1 binds the SMG1 C-terminal region through some part of the two RecA-like domains.

The SMG1 FRB Domain Recruits UPF2

We also reconstituted an SMG1C-UPF2 complex in vitro from purified SMG1C (49 nM final concentration) and recombinant UPF2 produced in *Escherichia coli* (1:3.5 molar ratio) (Figure S1). Processing of EM images obtained for this incubation revealed a mixture of species that included SMG1C-UPF2 complexes (20%) (Figures 5A and 5B). These complexes were enriched to a significant proportion (47%) after stabilization with a mild fixation, and 18,716 images were classified as SMG1C-UPF2 by image processing. UPF2 and SMG1C were mapped within the structure of SMG1C-UPF2 and solved at ~22 Å resolution (Figures 5C and 5D) after aligning and subtracting the structure of SMG1C to SMG1C-UPF2 (Figure 5E). UPF2 is recruited by the FRB domain of SMG1 at a proximal but distinct site to where UPF1 binds. UPF2 appeared in the complex as an open ring that could be fitted with three copies of a middle domain of eIF4G (MIF4G) (Kadlec et al., 2004) (cross correlation = 0.93), each end of the ring possibly corresponding to the N and C termini of UPF2, in agreement with previous data (Clerici et al., 2014; Melero et al., 2012) (Figure 5E). Only one of these ends contacted with SMG1, but the limited resolution impeded defining the three MIF4G domains in the structure. Then we analyzed the interaction of SBP-UPF2$^{2–775}$ (residues 2–775: comprising MIG4G1 and MIF4G2 domains) and SBP-UPF2$^{770–1272}$ (residues 770–1272: including MIF4G3 domain) (Figure S3) with Flag-HA-SBP-SMG1C (Figure 6A) and MBP-SMG1$^{1808–2743}$ (Figure 6B). These results suggested that both ends of UPF2 have the potential to recognize SMG1.

UPF1 and UPF2 Can Interact in the Context of SMG1C

The complex containing SMG1C, UPF1, and UPF2 was reconstituted in vitro by incubating purified SMG1C (14 nM final concentration) and the preassembled UPF1-UPF2 subcomplexes in a 1:4.5 molar ratio to favor the interaction, and the mixture was

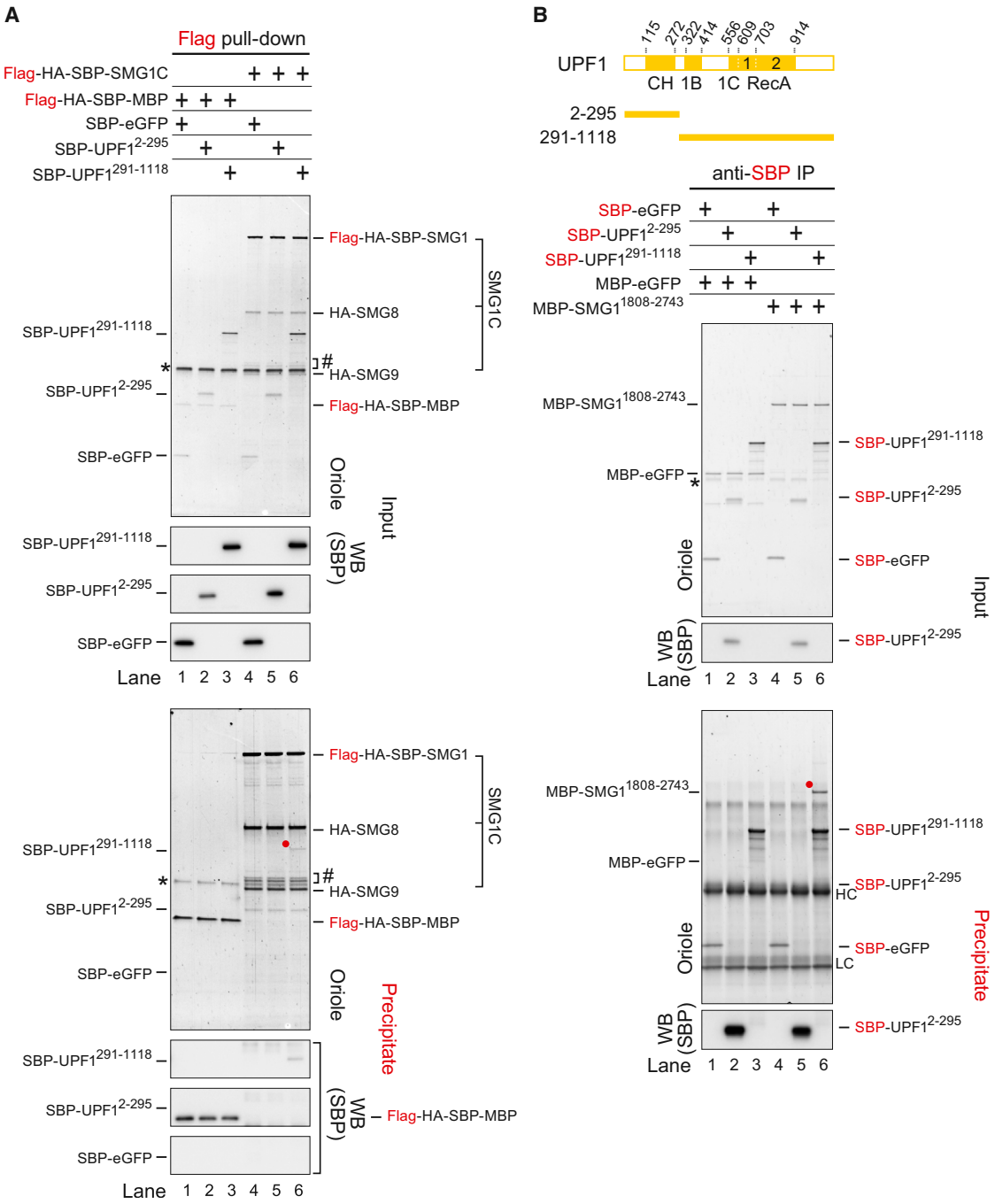

Figure 4. Interaction of N- and C-Terminal Fragments of UPF1 with SMG1C

(A) Pull-down assay testing the interaction of SMG1C and fragments of UPF1. Flag-HA-SBP-MBP (as control) or Flag-HA-SBP-SMG1C (30 nM each) were incubated with SBP-eGFP (as control), SBP-UPF1$^{2–295}$, and SBP-UPF1$^{291–1118}$ (90 nM each). A cartoon for these fragments can be seen in (B). Precipitated materials as well as 10% of input were subjected to SDS-PAGE and stained with Oriole stain; 10% of precipitated materials, as well as 1% of input, was analyzed by WB against the SBP tag.

(B) Pull-down assay testing the interaction of fragments of SMG1 and of UPF1. MBP-eGFP (as control) or MBP-SMG1$^{1808–2743}$ (90 nM each) were incubated with the SBP-eGFP (as control), SBP-UPF1$^{2–295}$, and SBP-UPF1$^{291–1118}$ (270 nM each); 10% of input and 150% of precipitated materials subjected to SDS-PAGE and stained with Oriole stain; 1% of input and 15% of precipitated materials were analyzed by WB.

Red dots, asterisk (*), hash (#), HC, and LC indicate the positions of coprecipitated proteins, BSA, uncharacterized contamination, IgG heavy chain, and IgG light chain, respectively (A and B). Preparation of the protein fragments used is shown in Figure S3.

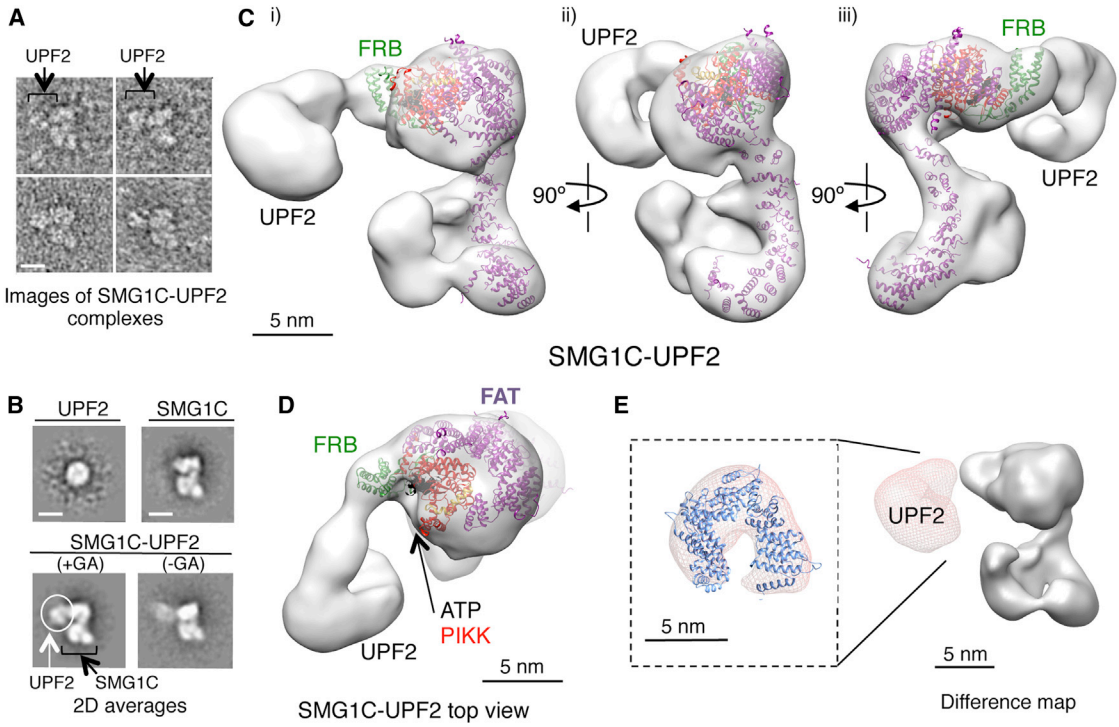

Figure 5. Structure of SMG1C-UPF2

(A) A gallery of four representative images of SMG1C-UPF2 complexes. The scale bar represents 10 nm.

(B) Representative 2D averages of UPF2, SMG1C, and SMG1C-UPF2. Averages of SMG1C-UPF2 obtained before and after a mild stabilization with glutaraldehyde (GA) are shown. The comparison of SMG1C, UPF2, and SMG1C-UPF2 identified UPF2 as a density bound to the head of SMG1, which has been highlighted within a circle. The scale bar represents 10 nm.

(C) Three approximately orthogonal views (labeled i, ii, and iii) of the EM structure of SMG1C-UPF2 (gray transparent density) fitted with segments of DNA-PKcs (Sibanda et al., 2010) and mTOR (Yang et al., 2013). The scale bar represents 5 nm.

(D) A top view of the SMG1C-UPF2 complex represented as in (C).

(E) Difference map obtained after subtracting SMG1C to SMG1C-UPF2, represented as a grid on the structure of SMG1C. The difference locates UPF2 in the complex, and this density was fitted with three copies of the crystal structure of the MIF4G3 domain (Kadlec et al., 2004).

analyzed by EM (Figure 7; Figure S1). We identified 32,918 images corresponding to SMG1C-UPF1-UPF2 by a combination of 2D and 3D classification in silico (details in Experimental Procedures). This subset behaved in image processing as a unique complex containing SMG1C and UPF1-UPF2 (Figures 7A and 7B). These images were used to determine the 3D structure of the complex, resolved at ~20 Å resolution (Figures 7C and 7D).

SMG1 and UPF1-UPF2 components were then positioned in SMG1C-UPF1-UPF2 after aligning and subtracting SMG1C to SMG1C-UPF1-UPF2 (Figure 7E), and the structural model for SMG1C was fitted within SMG1C-UPF1-UPF2 (Figures 7C and 7D; Movie S3). UPF1-UPF2 was mapped as a closed ring and an extension that could be fitted with a model of the UPF1-UPF2 complex (Melero et al., 2012) (Figures 7C and 7D). UPF2 comprises three conserved and homologous MIF4G domains organized as a distorted open ring (Clerici et al., 2014; Kadlec et al., 2004; Melero et al., 2012). For the model, we used three copies of the MIF4G3 domain (Kadlec et al., 2004) because the limited resolution did not allow resolving each MIF4G domain. The ring structure of UPF2 was a recognizable structural feature in the complex that did not contact SMG1C directly. The fitting of the UPF1-UPF2 model into SMG1C-UPF1-UPF2 predicted that UPF1 binds SMG1C through the RecA domains, which agrees with the biochemical data obtained (see below), and that UPF1 would be in an UPF2-bound open conformation (cross-correlation open versus closed conformation of UPF1 = 0.86 versus 0.75).

Our results showed that SMG1C could recruit UPF1 and UPF2 separately but also a preformed UPF1-UPF2 complex. Thus, we investigated whether SMG1C could bind both proteins separately but simultaneously and whether UPF1 and UPF2 could interact within the context of SMG1C. For this, we analyzed the competition of UPF1 and UPF2 for binding to SMG1C (Figure 8). Flag-HA-SBP-SMG1C) was preincubated with SBP-UPF1 or SBP-UPF2 to preassemble SMG1C-UPF1 or SMG1C-UPF2, respectively. The complex was pulled down using anti-Flag beads, and unbound SBP-UPF1 or SBP-UPF2 was washed out. Preassembled SMG1C-UPF1 or SMG1C-UPF2 complex was then incubated with increasing amounts of SBP-UPF2 or SBP-UPF1, respectively, and the amount of SBP-UPF2 and SBP-UPF1 retained by SMG1C was analyzed. SBP-UPF1 did not compete SBP-UPF2 from its complex with SMG1C, and SBP-UPF1 and SBP-UPF2 bound to SMG1C simultaneously (Figure 8A). On the other hand, SBP-UPF2, which could form a complex with SMG1C on its own (Figure 8B), competed with SBP-UPF1 for binding to SMG1C because increasing amounts

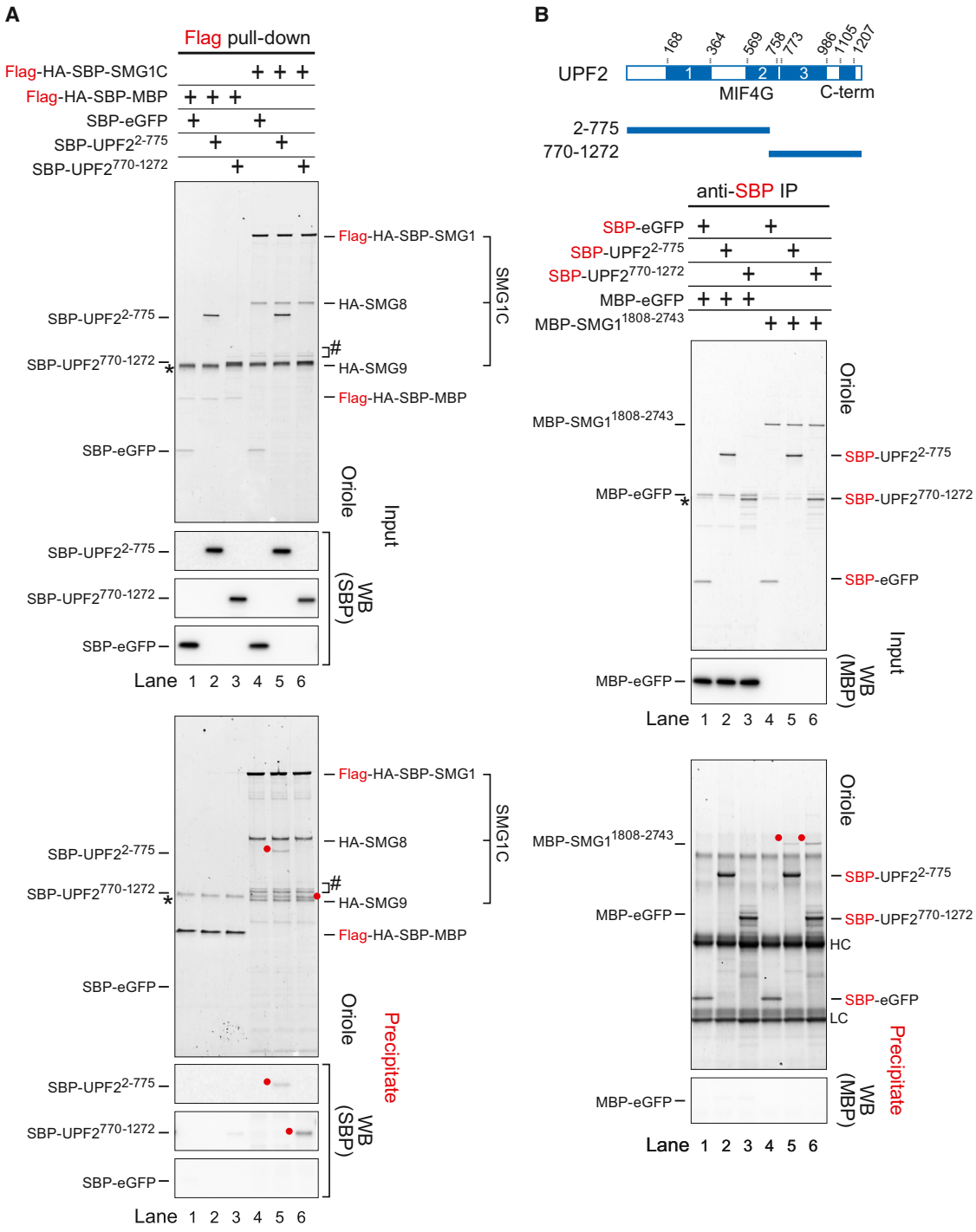

Figure 6. Interaction of N- and C-Terminal Fragments of UPF2 with SMG1C

(A) Pull-down assay testing the interaction of SMG1C and fragments of UPF2. Flag-HA-SBP-MBP (as control) or Flag-HA-SBP-SMG1C (30 nM each) was incubated with SBP-eGFP (as control), SBP-UPF2$^{2–775}$, and SBP-UPF2$^{770–1272}$ (90 nM each). A carton of these fragments is shown in (B). The input and precipitated samples were analyzed as described in Figure 4.

(B) Pull-down assay testing the interaction of fragments of SMG1 and of UPF2. MBP-eGFP (as control) or MBP-SMG1$^{1808–2743}$ (90 nM each) were incubated with SBP-eGFP (as control), SBP-UPF2$^{2–775}$, and SBP-UPF2$^{770–1272}$ (270 nM each). The input and the precipitated samples were analyzed as described in Figure 4. Red dots, asterisk (*), hash (#), HC, and LC are as described in Figures 4A and 4B. Preparation of the protein fragments used is shown in Figure S3.

See also Figure S3.

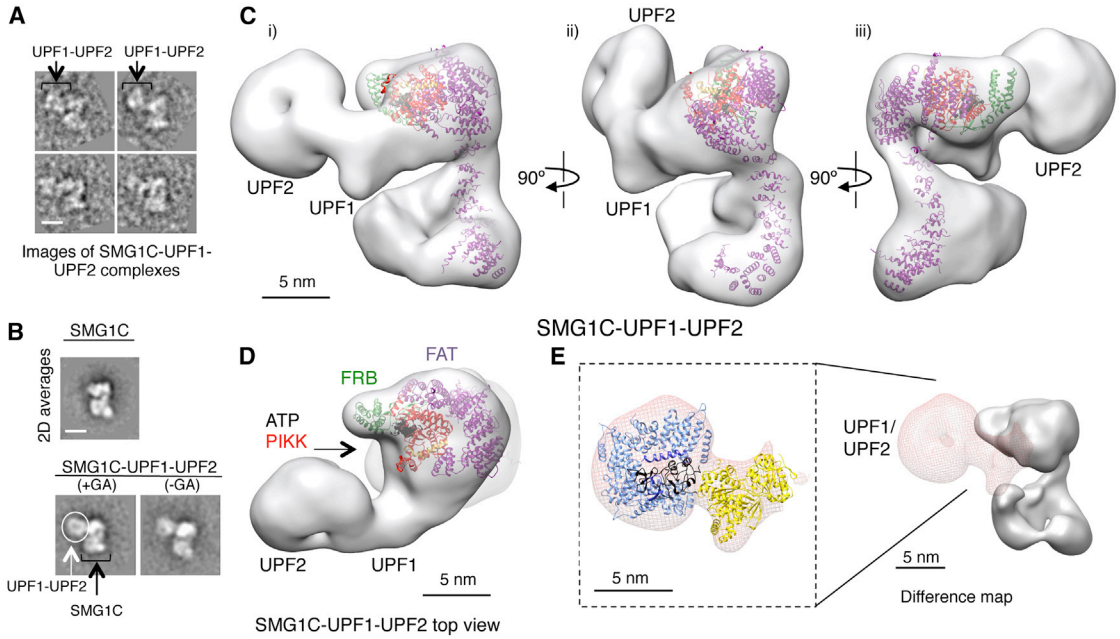

Figure 7. Structure of SMG1C-UPF1-UPF2

(A) EM images of the SMG1C-UPF1-UPF2 complex. The panel shows four representative images of SMG1C-UPF1-UPF2 complexes. The scale bar represents 10 nm.

(B) Representative 2D averages of images of the SMG1C-UPF1-UPF2 complex compared to an average of SMG1C. Averages before and after a mild stabilization with glutaraldehyde (GA) are also shown. The UPF1-UPF2 complex was identified as a density (highlighted within a circle) bound to SMG1C. The scale bar represents 10 nm.

(C) Three approximately orthogonal views (labeled i, ii, and iii) of the EM structure of SMG1C-UPF1-UPF2 (gray transparent density) fitted with segments of DNA-PKcs (Sibanda et al., 2010) and mTOR (Yang et al., 2013) crystal structures. The scale bar represents 5 nm.

(D) A top view of SMG1C-UPF1-UPF2 as in (C).

(E) Difference map obtained after subtracting SMG1C to SMG1C-UPF1-UPF2, represented as a grid on the structure of SMG1C. The difference locates UPF1-UPF2 in the complex, and this density could be fitted with a model of the UPF1-UPF2 complex (Clerici et al., 2014; Clerici et al., 2009; Melero et al., 2012) and using three copies of the crystal structure of the MIF4G3 domain (Kadlec et al., 2004). The CH domain of UPF1 bound to UPF2 is shown in black.

of SBP-UPF2 and decreasing amounts of SBP-UPF1 were detected in complex with Flag-HA-SBP-SMG1C (Figure 8C). Interestingly the double mutant UPF2-FE/ME, which does not bind UPF1 (Figure 1D), interacted with SMG1C (Figure 8B) but failed to compete out UPF1 (Figure 8C), and the interaction with SMG1C-UPF1 was greatly impaired. These results indicated that (1) UPF1 can be loaded to SMG1C-UPF2; (2) UPF2 can bind UPF1 in the context of the SMG1C complex, because only UPF2 that binds UPF1 competes this out from the complex, probably because once UPF1-UPF2 is formed, this complex disassembles from SMG1C; and (3) UPF2-FE/ME binds poorly to SMG1C when occupied by UPF1, indicating at least some partial obstruction for the simultaneous binding of UPF2 and UPF1 when they are not allowed to interact. As a whole, we interpreted these results as suggesting that UPF1 and UPF2 can interact in the context of SMG1C and that UPF2 in SMG1C-UPF2 can be transferred to UPF1 to assemble an SMG1C-UPF1-UPF2 complex.

DISCUSSION

We provide a structural model of SMG1, revealing the core architecture of this kinase, likely shared with other members of the PIKK family, such as ATM and ATR (Figure 2). The C terminus of SMG1 forms a compact globular structure with the catalytic and the FRB domains, forming a cleft where ATP binds and whose structure is, at low resolution, similar to the recently reported structure of mTOR (Yang et al., 2013). We propose that density in the SMG1 head that is not occupied by the structure of mTOR could correspond to the SMG1-specific insertion, which would be packed with the PIKK domain (Figure S2). The N terminus of SMG1 forms a helical scaffold protruding from the head. HEAT repeats function as protein interaction modules, and we do find that SMG8-SMG9 binds to this region. The comparison between SMG1 and DNA-PKcs uncovers interesting features of the PIKK family. SMG1 contains one helical arm with a similar helical twist as the proposed N-terminal arm of DNA-PKcs. The much-extended HEAT repeat regions in DNA-PKcs would account for its second arm, a likely adaptation to its functions in DNA repair (Sibanda et al., 2010). The precise orientation between the C-terminal region and the protruding arm in SMG1 is different from that of DNA-PKcs crystal structure, suggesting that this could vary within the PIKK family and/or during a functional cycle.

We show that SMG1, forming the SMG1C complex with SMG8 and SMG9, functions as a platform for the recruitment of UPF1 and UPF2 and that UPF1 and UPF2 can interact when in complex with SMG1C. We also found that when UPF1 and UPF2

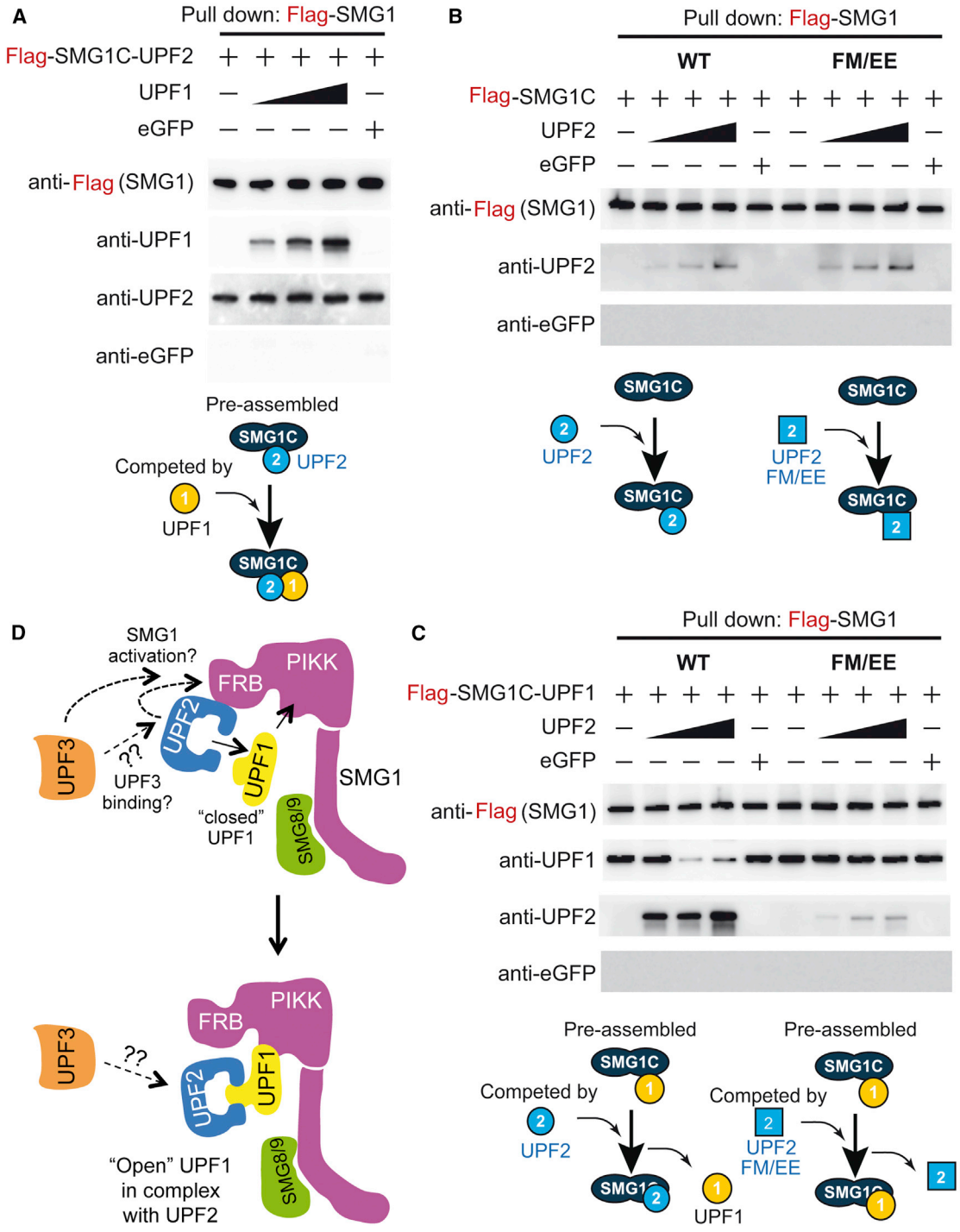

Figure 8. UPF1 and UPF2 Can Interact on the SMG1C

(A) Competition assay between SMG1C-UPF2 and UPF1. Flag-HA-SBP-SMG1C (30 nM) and SBP-UPF2 (90 nM) were mixed to form the SMG1C-UPF2 complex. The preassembled complexes were pulled down using anti-Flag beads. After washing out unbound UPF2, increasing amounts of SBP-UPF1 (0, 9, 30, and 90 nM) or control SBP-eGFP (90 nM) were added. The eluted proteins were analyzed by WB using the indicated antibodies.

(B) Binding activity of wild-type UPF2 (WT) or mutant UPF2 (FE/ME) to SMG1C. Flag-HA-SBP-SMG1C (30 nM) and increasing amounts of SBP-UPF2-WT (0, 9, 30, and 90 nM) or SBP-UPF2-FE/ME (0, 9, 30, and 90 nM), or control SBP-eGFP (90 nM) were mixed.

(C) Competition assay between SMG1C-UPF1 with UPF2 (WT or FE/ME). The procedure was as in (A), except that Flag-HA-SBP-SMG1C and SBP-UPF1 were mixed to form SMG1C-UPF1, and increasing amounts of SBP-UPF2-WT or SBP-UPF2-FE/ME were added for competition. Schematic representations of these experiments are shown (A)–(C).

(D) Possible model for the function of SMG1 as a platform for the recruitment of UPF1 and UPF2. UPF2 could bind SMG1-UPF1 directly or after its transfer from the FRB domain. Recruitment of UPF2 to FRB could contribute to activate SMG1, possibly with the contribution of UPF3.

are not allowed to interact (using UPF2-FE/ME), UPF1 partially obstructs UPF2 binding despite recognizing different regions in SMG1C, which may reflect some kind of steric clash because of their proximity. This in turn implies that the interaction of UPF1 to SMG1C-UPF2 probably occurs upon the transfer of UPF2 from SMG1C to UPF1 (Figure 8D). Other models could be conceivable if SMG1C-UPF1 is thought to assemble first. One possible scenario is that SMG1-UPF2 forms first, and then UPF1 binds to assemble an SMG1C-UPF1-UPF2 complex as the one we have resolved by EM. UPF2 binding to UPF1 within SMG1C would concomitantly release UPF2 from SMG1C because UPF2 would not be able to bind SMG1 and UPF1 simultaneously since both the N- and C-terminal ends in UPF2 participate in recognition of the UPF1 CH domain (Clerici et al., 2009; Melero et al., 2012). The structure of SMG1C-UPF1-UPF2 revealed that the interaction of UPF2 to UPF1 in the complex would promote an open conformation of UPF1 similar to that described in the crystal structure of UPF1 bound to the CH domain (Clerici et al., 2009).

UPF1 and UPF2 can also bind SMG1C independently because we can reconstitute SMG1C-UPF1 and SMG1-UPF2 in vitro. In addition, UPF1-C126S, which does not bind UPF2 (Kashima et al., 2006), and UPF2-FE/ME, which does not bind UPF1 (Figure 1D), also bind SMG1C in vivo. Furthermore, UPF1 knockdown did not affect the formation of a complex containing SMG1, UPF2, and Y14 (EJC component) (Kashima et al., 2006), and UPF2 knockdown increased the amount of the SURF complex, containing SMG1 and UPF1 in vivo (Kashima et al., 2006). Consistently, EM structures of SMG1C-UPF1 and SMG1C-UPF2 revealed that each protein recognizes distinct sites in SMG1. UPF1 is recruited to the proximities of the SMG1 catalytic domain, and the low-resolution structure of UPF1 bound to SMG1C matches better the helicase inactive form of UPF1 (Chakrabarti et al., 2011) than the active open conformation (Clerici et al., 2009). Based on these results, we propose that UPF1 is recruited to SMG1 in a closed and inactive conformation. On the other hand, the FRB domain in SMG1 recruits UPF2, and interestingly the FRB domain in mTOR binds S6K1, an mTOR substrate, enhancing its phosphorylation. UPF2 when bound to SMG1 appears as an open ring similar to the low-resolution structures of UPF2 described before (Melero et al., 2012), with each end of the ring representing the N- and C-terminal side of UPF2. Only one of the two ends is bound to SMG1, but our biochemical experiments using N- and C-terminally truncated versions of UPF2 showed that both truncated mutants could interact with SMG1. We cannot rule out that these interactions represent different complexes between UPF2 and SMG1. Consistently, the C-terminal MIF4G3 domain of UPF2 has been shown to bind SMG1 in vitro (Clerici et al., 2014).

The structure of mTOR suggested that recruitment of substrates to the PIKK domain could be the main mechanism to control phosphorylation and that the FRB domain appeared to regulate phosphorylation by facilitating access to the active site (Yang et al., 2013). The structures of the SMG1C-UPFs suggest that the mTOR model could be, at least in some aspects, extended to SMG1. UPF2 and UPF3 are required to activate UPF1 phosphorylation by SMG1 in vivo because UPF1 mutants that bind SMG1 but cannot associate with UPF2 are poorly phosphorylated by SMG1 in mammalian cells (Ivanov et al., 2008; Kashima et al., 2006). UPF2 is recruited to the FRB, and this interaction could maybe contribute to activate SMG1. However, additional signals appear to be required to trigger phosphorylation in SMG1. Phosphorylation of UPF1 is downmodulated by SMG8-SMG9 (Arias-Palomo et al., 2011; Yamashita et al., 2009). SMG8 induces a large rotation of the N-terminal arm, a conformational change that parallels other HEAT repeat containing proteins after ligand binding (Figure 2; Movies S1 and S2). The mechanism of regulation may be indirect because we do not find an obvious contact between SMG8-SMG9 and the kinase region. In addition, UPF2 mutants that bind UPF1 and SMG1 but not UPF3 suppressed UPF1 phosphorylation (Kashima et al., 2006). UPF3 and/or the UPF3-EJC complex binding to this complex might induce the conformational changes required for SMG1 activation. The structures of SMG1C-UPFs, if interpreted in the context of those models that propose that the EJC stimulates UPF1 phosphorylation, would suggest that SMG1C would be bound to UPF1 as part of SURF, and SURF would then interact with UPF2-UPF3-EJC to assemble one or several transient structural intermediates. SMG1 would bind UPF1 and UPF2 simultaneously within these complexes, and it would facilitate UPF2 binding to UPF1, whereas the interaction of UPF2 and/or UPF2-UPF3 with SMG1 would activate this kinase and UPF1 phosphorylation (Kashima et al., 2006; Yamashita et al., 2009). Indeed, it has been shown that an SMG1-UPF2/UPF3b complex can be formed in vitro (Clerici et al., 2014). On the other hand, some evidence suggests that distinct but related pathways rather than only one mechanism could activate NMD, including EJC-independent pathways. SMG1C could maybe potentially serve as a platform for an UPF2-dependent activation of UPF1 without the need for an EJC.

EXPERIMENTAL PROCEDURES

Plasmids and Antibodies

pEF_Flag-HA-SBP-SMG1 (residues 1–3657), pSR_Strep-HA-SMG9 (residues 2–520), pSR_Strep-HA-SMG8 (residues 2-991), pSR_HA-UPF1, siLentGene-puro-siSMG8cds, siLentGene-puro-siSMG9cds, and siLentGene-puro-siUPF1cds plasmids were described previously (Kashima et al., 2006; Usuki et al., 2013; Yamashita et al., 2009). pEFh_SBP-UPF1 (residues 2–1118, codon optimized), pEFh_SBP-UPF2 (residues 2-1272), pEFh_SBP-UPF2-E858R (residues 2–1272, E858R), pEFh_SBP-UPF2-F1113E-M1173E, pEFh_SBP-UPF1$^{2-295}$ (residues 2-295, codon optimized), pEFh_SBP-UPF1$^{291–1118}$ (residues 291–1118, codon optimized), pEFh_SBP-UPF2$^{2-775}$ (residues 2-775, codon optimized), pEFh_SBP-UPF2$^{770–1272}$ (residues 770–1272, codon optimized), pEFh_SBP-eGFP (codon optimized), pEF_Flag-HA-SBP-MBP, pEFh_MBP-SMG1$^{1808–2743}$ (residues 1808–2743, codon optimized), and pEFh_MBP-eGFP plasmids were constructed cloning each cDNA fragment following standard methods.

Antibodies against SMG1, SMG8, SMG9, UPF1, UPF2, UPF3a, and UPF3b were described previously (Kashima et al., 2006; Yamashita et al., 2009). Antibodies against eIF4A3 (ProteinTech), Flag (M2; Sigma), SBP (SB19-C4; Santa Cruz), and MBP (NEB) were obtained commercially. Fab fragments of SMG8 generated from SMG8 polyclonal antibodies were generated using the Pierce Fab Micro Preparation Kit.

Purification of Proteins and Protein Complexes

SBP-UPF1, SBP-UPF2, SBP-UPF2-F1113E-M1173E, the SBP-UPF2:HA-UPF1 complex (used in Figure 1), the SBP-UPF2-E858R:HA-UPF1 complex (used in Figure 7), SBP-UPF1$^{2-295}$, SBP-UPF1$^{291–1118}$, SBP-UPF2$^{2–775}$, SBP-UPF2$^{770–1272}$, Flag-HA-SBP-SMG1 (residues 126–3,657), Flag-HA-SBP-SMG1C, Flag-HA-SBP-MBP, SBP-eGFP, MBP-eGFP, and

MBP-SMG1$^{1808–2743}$ were purified as described before (Arias-Palomo et al., 2011). In brief, 3 × 10^7 to 6 × 10^8 of 293T cells were cotransfected with plasmids encoding protein listed above using LipofectaminLTX (Life Technologies) or polyethyleneimine (Polysciences). During purification of SMG1, potential contamination by SMG8 and SMG9 was avoided by cotransfection of siLentGene-puro-siSMG8cds and siLentGene-puro-siSMG9cds and by immune affinity using antibodies against these two proteins. Similarly, during purification of UPF2, UPF2-E858R, and UPF2$^{770–1272}$, potential contaminations by UPF1 and UPF3 were avoided by cotransfection of siLentGene-puro-siUPF1cds and immune affinity using antibodies against UPF1, UPF3a, and UPF3b. Two to three days after transfection, cells were lysed with a loose-fit Potter-Elvehjem Homogenizer in NF buffer (20 mM Tris-HCl [pH 7.5], 150 mM NaCl, 0.25 M sucrose, 0.5% NP40, 1% Tween 20, 1 mM dithiothreitol [DTT], protease inhibitor cocktail [Nacalai Tesque], phosphatase inhibitor cocktail [EDTA free; Nacalai Tesque]) containing 50 μg/ml RNase A. SBP- or MBP-tagged proteins were captured by streptavidin Mag Sepharose (GE Healthcare) or Amylose Magnetic Beads (NEB), respectively. After washing with NF buffer, the affinity-purified protein complexes were eluted by incubation at 4°C for 30 min with T buffer (20 mM HEPES-KOH [pH 7.5], 150 mM NaCl, 2.5 mM $MgCl_2$, 0.05% Tween 20) containing 2 mM DTT, protease inhibitor cocktail (EDTA free; Nacalai Tesque), phosphatase inhibitor cocktail (Nacalai Tesque), and 2 mM biotin (for SBP; Sigma) or 20 mM maltose (for MBP), respectively. Eluted proteins were separated by SDS-PAGE and were stained with Oriole fluorescent gel stain (Bio-Rad). Oriole-stained protein signals were quantified with a Lumino-Imager, LAS-4000, and Science Lab Image Gauge software (Fuji Photo Film). For the reconstitution of SMG1C-UPF2 complex to be analyzed in EM, we used purified UPF2 (kindly provided by Elena Conti, Max Planck Institut) corresponding to the same preparation used before for EM (Melero et al., 2012).

WB Analysis

All western blot (WB) experiments were detected with the ECL western blotting detection kit (GE Biotech), Luminata Classico Western HRP substrate (Millipore), Luminata Forte Western HRP substrate (Millipore), or ImmunoStar LD (Wako) using a LuminoImager, LAS-4000, and Science Lab 2001 Image Gauge software (Fuji Photo Film).

Pull-Down Assays Using the SBP-Tagged Version of UPF2 from HeLa TetOff Cells and WB Analysis

HeLa TetOff cells were transfected within indicated plasmids using Lipofectamine LTX (Invitrogen). Two days after transfection, cells were lysed with a loose-fit Potter-Elvehjem homogenizer in T buffer containing 50 μg/ml RNase A. SBP-tagged proteins were pulled down by streptavidin Mag Sepharose (GE Healthcare). After washing with T buffer, the Mag Sepharose was eluted by 2 mM biotin, and 2× SDS sample buffer was added. Eluted proteins were separated by SDS-PAGE and were probed by the indicated antibodies. Experiments were performed three times, and typical results are shown.

EM and Image Processing

Complexes were assembled after incubating SMG1C with UPF1, UPF2, or UPF1-UPF2 at 25°C for 30 min in an excess of UPFs compared with SMG1C as indicated in Figure S1. For some experiments, the complexes were mildly stabilized by incubating the mixture at 25°C for another 10 min in the presence of 0.02% glutaraldehyde. Samples of SMG1 and SMG1C and the incubations of SMG1C with UPF1, UPF2, and UPF1-UPF2 were adsorbed on carbon-coated grids and stained using 1% uranyl formate. Observations were performed using a JEOL-1230 at 100 kV, and images were collected by an automatic data collection scheme using a TVIPS F416 CMOS and a final magnification of 54,926. CTF for all micrographs were corrected using BSOFT (Heymann and Belnap, 2007). Some images were also collected at 20° tilting to increase the number of views during image processing. Images of individual molecules in all samples were extracted automatically and subsequently classified and averaged by a combination of maximum-likelihood methods (Scheres et al., 2007), classification methods implemented in XMIPP (Sorzano et al., 2004), and a multireference supervised classification. In brief, 2D averaging and classification was used to identify and removed those images corresponding to small particles (likely free UPF1, UPF2 or UPF1-UPF2) and define a subset of SMG1C-contaning complexes. Subsequently, images corresponding to free SMG1C and the complexes were further identified and classified in a 3D processing strategy using maximum-likelihood methods (Scheres et al., 2007) and supervised classifications. Supervised classifications were performed by comparing each SMG1C-like image to all projections from several 3D templates including SMG1 and SMG1C. After classification, we isolated a subset of images corresponding to a homogenous structural complex containing SMG1C bound to UPFs that behaved as a unique structure during refinement (at the resolution of these studies) because the data set could not be classified further using maximum-likelihood methods (Scheres et al., 2007). Details on the number of images for each step can be found in Figure S1B. After classification, images of SMG1, SMG1C, SMG1C-UPF1, SMG1C-UPF2, and SMG1C-UPF1-UPF2 were processed independently. Images were refined using EMAN (Ludtke et al., 1999; Ludtke, 2010). Templates for refinement were obtained using the volume generator from EMAN2. The resolution of the structures was estimated using the Fourier shell correlation method and a 0.5 correlation coefficient. These estimates were 21.9, 20.8, 21.0, 21.7, and 19.5 Å for SMG1, SMG1C, SMG1C-UPF1, SMG1C-UPF2, and SMG1C-UPF1-UPF2, respectively (Figure S2).

Difference maps between SMG1C and SMG1, as well as SMG1C and the several SMG1C-UPF complexes, were carried out by alignment the corresponding 3D structures and a subtraction using UCSF Chimera (Goddard et al., 2007). Fitting of atomic structures corresponding to the crystal structures of DNA-PKcs (Protein Data Bank [PDB] ID 3KGV) (Sibanda et al., 2010), mTOR (PDB ID 4JSP) (Yang et al., 2013), UPF1 (PDB ID 2XZL and 2WJV) (Chakrabarti et al., 2011; Clerici et al., 2009), a MIF4G3 domain (Kadlec et al., 2004), and a model of UPF2 (Melero et al., 2012) was performed using UCSF Chimera (Goddard et al., 2007). The handedness of the reconstructions was determined by the fitting of the C-terminal region of the crystal structure of mTOR into the head region of SMG1. For the immunolabeling experiment, Fab fragments directed against SMG8 were incubated with SMG1C, and the immune complexes were observed in the electron microscope and processed in 2D as described for the rest of the complexes.

Modeling Conformational Transition from SMG1 to SMG1C

The movement that takes place from SMG1 to SMG1C can be modeled using UCSF Chimera (Goddard et al., 2007), and Figure 2H and Movie S1 represent several possible transient states. SMG1 and SMG1C are showed slightly tilted to help visualizing the conformational change.

In Vitro Protein-Binding Experiments

In vitro pull-down assays were performed in T buffer [20 mM HEPES-KOH (pH 7.5), 150 mM NaCl, 2.5 mM $MgCl_2$, 0.05% Tween 20] complemented with 1 mM $MgCl_2$, 1 mM $MnCl_2$, 1 μM $ZnCl_2$, 1 mM DTT, and 0.0025% (for Flag pull-down) or 0.005% BSA (for SBP pull-down) at 4°C. For Flag pull-down assays, 30 nM Flag-HA-SBP-eGFP and Flag-HA-SBP-SMG1C were incubated with the following proteins (90 nM each): SBP-eGFP (Figures 1C, 4A, and 6A); SBP-UPF1, SBP-UPF2 and SBP-UPF2:HA-UPF1 (Figure 1); SBP-UPF1$^{2–295}$ and SBP-UPF1$^{291–1118}$ (Figure 4A); and SBP-UPF2$^{2–775}$ and SBP-UPF2$^{770–1272}$ (Figure 6A). For SBP pull-down assays, 90 nM MBP-eGFP and MBP-SMG1$^{1807–2743}$ were incubated with the following proteins (270 nM each): SBP-eGFP (Figures 4B and 6B); SBP-UPF1$^{2–295}$ and SBP-UPF1$^{291–1118}$ (Figure 6B); and SBP-UPF2$^{2-775}$ and SBP-UPF2$^{770–1272}$ (Figure 6B). After 3 hr incubation, the mixtures were added to the anti-Flag-M2 Magnetic Beads (Sigma) or anti-SBP (SB19-C4, SantaCruz) antibody-immobilized Dynabeads protein G (Invitrogen) and incubated for 2 hr, and the beads were washed four times with T buffer containing 1 mM DTT. The bound proteins were eluted with T buffer containing 1 mM DTT and 150 μg/ml 3X Flag peptide (Sigma) (for Flag pull-down) or SDS sample buffer (for SBP pull-down). The eluted proteins were analyzed by SDS-PAGE and stained with Oriole stain, and WB.

In Vitro Competition Assays

Experiments were performed in T buffer complemented with 1 mM $MgCl_2$, 1 mM $MnCl_2$, 1 μM $ZnCl_2$, 1 mM DTT, and 0.0025% BSA at 4°C. To prepare the preassembled complexes, 30 nM Flag-HA-SBP-SMG1C was mixed with 90 nM SBP-UPF1 or SBP-UPF2 and incubated for 3 hr, and the preassembled

complexes were pulled down by Flag-M2 magnetic beads (Sigma). The beads were washed four times with T buffer containing 1 mM DTT. Then the washed beads were incubated with the following proteins for 1 hr: 90 nM SBP-eGFP; 0, 9, 30 and 90 nM SBP-UPF2; and 0, 9, 30 and 90 nM SBP-UPF2-F1113E-M1173E or 0, 9, 30 and 90 nM SBP-UPF1. Following incubation, the beads were as described above, and the bound proteins were eluted with T buffer containing 1 mM DTT and 150 μg/ml 3X Flag peptide (Sigma). The eluted proteins were analyzed by SDS-PAGE and stained with Oriole stain and WB.

ACCESSION NUMBERS

The EM maps have been deposited in the EM database with accession numbers EMD-2662 (for SMG1), EMD-2663 (for SMG1C), EMD-2664 (for SMG1C-UPF1), EMD-2665 (for SMG1C-UPF2), and EMD-2666 (for SMG1C-UPF1-UPF2).

SUPPLEMENTAL INFORMATION

Supplemental Information includes three figures and three movies and can be found with this article online at http://dx.doi.org/10.1016/j.str.2014.05.015.

AUTHOR CONTRIBUTIONS

A.Y. and O.L. planned the project and wrote most of the manuscript. R.M. performed all the microscopy and image processing. A.U. performed all biochemical analysis. A.U. and H.K. purified most proteins. R.C. helped with the purification of proteins. N.K. contributed with the *in vitro* analyses. S.O. helped in the design and synthesis of SMG1, SMG8, SMG9, UPF1, and UPF2 constructs.

ACKNOWLEDGMENTS

We thank Elena Conti and her team (Max Planck Institut) for providing UPF2 and suggestions, Jasminka Boskovic (CNIO, Madrid) for critically reading this manuscript, and Ernesto Arias-Palomo for suggestions. This work was supported by the Spanish Government (SAF2011-22988 to O.L., Juan de la Cierva contract JCI-2011-09536 to R.M., RD06/0020/1001 from the Instituto de Salud Carlos III to O.L., and contract to R.C.); the Japan Society for the Promotion of Science KAKENHI (grants 23687025, 23112718, and 21115004 to A.Y.); the Takeda Science Foundation (to A.Y.); and the Ministry of Education, Culture, Sports, Science and Technology of Japan (Grant-in-Aid for Scientific Research on Innovative Areas no. 23112706 to N.K.).

Received: April 28, 2014
Revised: May 27, 2014
Accepted: May 27, 2014
Published: July 3, 2014

REFERENCES

Arias-Palomo, E., Yamashita, A., Fernández, I.S., Núñez-Ramírez, R., Bamba, Y., Izumi, N., Ohno, S., and Llorca, O. (2011). The nonsense-mediated mRNA decay SMG-1 kinase is regulated by large-scale conformational changes controlled by SMG-8. Genes Dev. *25*, 153–164.

Chakrabarti, S., Jayachandran, U., Bonneau, F., Fiorini, F., Basquin, C., Domcke, S., Le Hir, H., and Conti, E. (2011). Molecular mechanisms for the RNA-dependent ATPase activity of Upf1 and its regulation by Upf2. Mol. Cell *41*, 693–703.

Clerici, M., Mourão, A., Gutsche, I., Gehring, N.H., Hentze, M.W., Kulozik, A., Kadlec, J., Sattler, M., and Cusack, S. (2009). Unusual bipartite mode of interaction between the nonsense-mediated decay factors, UPF1 and UPF2. EMBO J. *28*, 2293–2306.

Clerici, M., Deniaud, A., Boehm, V., Gehring, N.H., Schaffitzel, C., and Cusack, S. (2014). Structural and functional analysis of the three MIF4G domains of nonsense-mediated decay factor UPF2. Nucleic Acids Res. *42*, 2673–2686.

Franks, T.M., Singh, G., and Lykke-Andersen, J. (2010). Upf1 ATPase-dependent mRNP disassembly is required for completion of nonsense- mediated mRNA decay. Cell *143*, 938–950.

Glavan, F., Behm-Ansmant, I., Izaurralde, E., and Conti, E. (2006). Structures of the PIN domains of SMG6 and SMG5 reveal a nuclease within the mRNA surveillance complex. EMBO J. *25*, 5117–5125.

Goddard, T.D., Huang, C.C., and Ferrin, T.E. (2007). Visualizing density maps with UCSF Chimera. J. Struct. Biol. *157*, 281–287.

Hansen, K.D., Lareau, L.F., Blanchette, M., Green, R.E., Meng, Q., Rehwinkel, J., Gallusser, F.L., Izaurralde, E., Rio, D.C., Dudoit, S., and Brenner, S.E. (2009). Genome-wide identification of alternative splice forms down-regulated by nonsense-mediated mRNA decay in Drosophila. PLoS Genet. *5*, e1000525.

Heymann, J.B., and Belnap, D.M. (2007). Bsoft: Image processing and molecular modeling for electron microscopy. J. Struct. Biol. *157*, 3–18.

Ivanov, P.V., Gehring, N.H., Kunz, J.B., Hentze, M.W., and Kulozik, A.E. (2008). Interactions between UPF1, eRFs, PABP and the exon junction complex suggest an integrated model for mammalian NMD pathways. EMBO J. *27*, 736–747.

Izumi, N., Yamashita, A., and Ohno, S. (2012). Integrated regulation of PIKK-mediated stress responses by AAA+ proteins RUVBL1 and RUVBL2. Nucleus *3*, 29–43.

Kadlec, J., Izaurralde, E., and Cusack, S. (2004). The structural basis for the interaction between nonsense-mediated mRNA decay factors UPF2 and UPF3. Nat. Struct. Mol. Biol. *11*, 330–337.

Kashima, I., Yamashita, A., Izumi, N., Kataoka, N., Morishita, R., Hoshino, S., Ohno, M., Dreyfuss, G., and Ohno, S. (2006). Binding of a novel SMG-1-Upf1-eRF1-eRF3 complex (SURF) to the exon junction complex triggers Upf1 phosphorylation and nonsense-mediated mRNA decay. Genes Dev. *20*, 355–367.

Kervestin, S., and Jacobson, A. (2012). NMD: A multifaceted response to premature translational termination. Nat. Rev. Mol. Cell Biol. *13*, 700–712.

Loh, B., Jonas, S., and Izaurralde, E. (2013). The SMG5-SMG7 heterodimer directly recruits the CCR4-NOT deadenylase complex to mRNAs containing nonsense codons via interaction with POP2. Genes Dev. *27*, 2125–2138.

Ludtke, S.J. (2010). 3-D structures of macromolecules using single-particle analysis in EMAN. Methods Mol. Biol. *673*, 157–173.

Ludtke, S.J., Baldwin, P.R., and Chiu, W. (1999). EMAN: Semiautomated software for high-resolution single-particle reconstructions. J. Struct. Biol. *128*, 82–97.

Melero, R., Buchwald, G., Castaño, R., Raabe, M., Gil, D., Lázaro, M., Urlaub, H., Conti, E., and Llorca, O. (2012). The cryo-EM structure of the UPF-EJC complex shows UPF1 poised toward the RNA 3′ end. Nat. Struct. Mol. Biol. *19*, 498–505, S1–S2.

Mendell, J.T., Sharifi, N.A., Meyers, J.L., Martinez-Murillo, F., and Dietz, H.C. (2004). Nonsense surveillance regulates expression of diverse classes of mammalian transcripts and mutes genomic noise. Nat. Genet. *36*, 1073–1078.

Okada-Katsuhata, Y., Yamashita, A., Kutsuzawa, K., Izumi, N., Hirahara, F., and Ohno, S. (2012). N- and C-terminal Upf1 phosphorylations create binding platforms for SMG-6 and SMG-5:SMG-7 during NMD. Nucleic Acids Res. *40*, 1251–1266.

Scheres, S.H., Gao, H., Valle, M., Herman, G.T., Eggermont, P.P., Frank, J., and Carazo, J.M. (2007). Disentangling conformational states of macromolecules in 3D-EM through likelihood optimization. Nat. Methods *4*, 27–29.

Schweingruber, C., Rufener, S.C., Zünd, D., Yamashita, A., and Mühlemann, O. (2013). Nonsense-mediated mRNA decay: Mechanisms of substrate mRNA recognition and degradation in mammalian cells. Biochim. Biophys. Acta *1829*, 612–623.

Shigeoka, T., Kato, S., Kawaichi, M., and Ishida, Y. (2012). Evidence that the Upf1-related molecular motor scans the 3′-UTR to ensure mRNA integrity. Nucleic Acids Res. *40*, 6887–6897.

Sibanda, B.L., Chirgadze, D.Y., and Blundell, T.L. (2010). Crystal structure of DNA-PKcs reveals a large open-ring cradle comprised of HEAT repeats. Nature *463*, 118–121.

Sorzano, C.O., Marabini, R., Velázquez-Muriel, J., Bilbao-Castro, J.R., Scheres, S.H., Carazo, J.M., and Pascual-Montano, A. (2004). XMIPP: A

new generation of an open-source image processing package for electron microscopy. J. Struct. Biol. *148*, 194–204.

Usuki, F., Yamashita, A., Shiraishi, T., Shiga, A., Onodera, O., Higuchi, I., and Ohno, S. (2013). Inhibition of SMG-8, a subunit of SMG-1 kinase, ameliorates nonsense-mediated mRNA decay-exacerbated mutant phenotypes without cytotoxicity. Proc. Natl. Acad. Sci. USA *110*, 15037–15042.

Weischenfeldt, J., Waage, J., Tian, G., Zhao, J., Damgaard, I., Jakobsen, J.S., Kristiansen, K., Krogh, A., Wang, J., and Porse, B.T. (2012). Mammalian tissues defective in nonsense-mediated mRNA decay display highly aberrant splicing patterns. Genome Biol. *13*, R35.

Yamashita, A. (2013). Role of SMG-1-mediated Upf1 phosphorylation in mammalian nonsense-mediated mRNA decay. Genes Cells *18*, 161–175.

Yamashita, A., Ohnishi, T., Kashima, I., Taya, Y., and Ohno, S. (2001). Human SMG-1, a novel phosphatidylinositol 3-kinase-related protein kinase, associates with components of the mRNA surveillance complex and is involved in the regulation of nonsense-mediated mRNA decay. Genes Dev. *15*, 2215–2228.

Yamashita, A., Izumi, N., Kashima, I., Ohnishi, T., Saari, B., Katsuhata, Y., Muramatsu, R., Morita, T., Iwamatsu, A., Hachiya, T., et al. (2009). SMG-8 and SMG-9, two novel subunits of the SMG-1 complex, regulate remodeling of the mRNA surveillance complex during nonsense-mediated mRNA decay. Genes Dev. *23*, 1091–1105.

Yang, H., Rudge, D.G., Koos, J.D., Vaidialingam, B., Yang, H.J., and Pavletich, N.P. (2013). mTOR kinase structure, mechanism and regulation. Nature *497*, 217–223.